Post-Composition Primal-Dual Algorithm for Texture, Geometry, and Noise Separation

Adrien Meynard[1] , Nelly Pustelnik[1], Luis Briceño-Arias[2] and Sylvain Meignen[3]
[1] *ENS de Lyon, CNRS, LPENSL, UMR5672, Lyon, France*
[2] *Universidad Técnica Federico Santa María, Departamento de Matemática, Santiago, Chile*
[3] *University Grenoble Alpes, CNRS, Jean Kuntzmann Laboratory, Grenoble, France*
adrien.meynard@ens-lyon.fr, nelly.pustelnik@ens-lyon.fr, luis.briceno@usm.cl, sylvain.meignen@univ-grenoble-alpes.fr

***Abstract*—In this paper, we propose a new algorithm for separating geometry and texture in noisy images. The proposed algorithm uses a novel primal-dual approach exploiting post-composition. We show that the latter exhibits significantly better computational performance than standard forward-backward iterations and provides a more flexible formulation, opening the door to future integration with proximal neural networks.**

***Index Terms*—texture geometry image decomposition, primal-dual approaches, variational techniques**

I. Introduction

Image denoising, and more generally image restoration, has made significant advances in recent years, with a consensus now being reached on model-based neural network approaches [1], [2]. However, these approaches show that the underlying structure of variational problem and associated algorithms are of considerable importance. In particular, designing fast algorithms for image restoration tasks makes it then possible to obtain efficient unfolded methods [3]. In the present contribution, our analysis focuses on the standard variational formulation, putting the texture-geometry decomposition approach back into a sufficiently flexible framework and deriving a suitable and efficient algorithmic implementation, leading to solid building blocks for future unfolded framework.

State-of-the-art. In image restoration problems, one traditionally assumes an image is a bounded variation function plus some noise, leading to the very popular Rudin-Osher-Fatemi (ROF) restoration model [4]. However, Meyer pointed out in [5] that images may contain some strong oscillations, not taken into account in the ROF model. Instead, images should rather be viewed as the superimposition of three components: geometry (bounded variation), texture (strong oscillations), and noise. For that purpose, considering noiseless images, a first approach to separate geometry and texture was proposed in [6], where the minimization problem is formulated in terms of the bounded variation operator and its dual. In that paper, the texture and geometry components of the image are computed using projection on convex sets, inspired by the work of Chambolle [7]. Other approaches were also proposed to implement this new decomposition scheme, as in [8] where the ROF model was modified to find the optimal image decomposition by formally solving the Euler-Lagrange equation. The approach detailed in [6] can be generalized by changing the total variation into L^p-norms or wavelet decomposition, leading to different dual norms controlling the texture component [9]. Additionally, it can incorporate noise, assumed to be Gaussian white [10].

This work was supported in part by the DECIMA project from University Grenoble Alpes. This work is funded by the Fondation Simone et Cino Del Duca - Institut de France.

Contribution. In the present paper, we first recall the general minimization context and then show that the proposed minimization problem can be embedded in a more general framework. We then introduce iterations based on a forward-backward approach, and then explain how by rewriting the minimization problem using post-composition, the minimum can also be found by adapting the Condat-Vũ algorithm [11], [12]. Throughout different simulations, we emphasize that the proposed primal-dual algorithm provides computational gain over the forward-backward approach. The algorithmic procedure being fast enough, it allows us to evaluate the impact of the involved regularization parameters on the solution.

Notations. In this paper, we consider an image z of size $N \times N$, X denotes $\mathbb{R}^{N\times N}$, and $Y = X \times X$. The Euclidean norm in $\mathbb{R}^2$ is denoted by $\|\cdot\|_2$.

II. Texture + Geometry Formulation

A. Standard Formulation

Image decomposition is often performed by considering that an image is the superimposition of some texture and cartoon parts, the first one living in a space of oscillations and the second being modelled as a bounded variation function [6].

To define the set of bounded variation functions, the discrete total variation is introduced as follows:

$$(\forall x \in X) \quad J(x) = \sum_{1\leq i,j\leq N} \|(Lx)_{i,j}\|_2. \tag{1}$$

where L denotes the bi-dimensional finite differences operator. To model the oscillations, we introduce the subspace

$$G = \{y \in X, \exists g \in Y \text{ s.t } y = \mathrm{div}(g)\}, \tag{2}$$

where div denotes the discrete divergence. This space is equipped with the norm:

$$\|y\|_G = \inf\left\{\|g\|_\infty = \max_{i,j}\|g_{i,j}\|_2,\ y = \mathrm{div}(g), g \in Y\right\}. \tag{3}$$

The subset C_μ contains the elements of G with a norm smaller than μ. Given an image z, its decomposition into a bounded variation function x and a texture component y is performed by solving the following minimization problem [13]:

$$\min_{(x,y)\in X\times C_\mu} \frac{1}{2}\|z-x-y\|_2^2 + \lambda J(x). \tag{4}$$

B. Duality

It is well known that [13]:

$$J(x) = \sup_{v\in C_1} \langle x, v\rangle_X. \tag{5}$$

Using the Legendre-Fenchel transformation, one obtains that (4) can be rewritten as:

$$\min_{(x,y)\in Y} \frac{1}{2}\|z-x-y\|_2^2 + \lambda J(x) + J^*\Big(\frac{y}{\mu}\Big). \tag{6}$$

The parameter μ determines the frequency content assigned to the texture part y: a smaller μ results in the inclusion of higher-frequency oscillations in the texture [10]. The formulation of the minimization problem proposed in (6) has paved the way to a more general setting to texture and geometry separation. Indeed, by setting $p > 1$ and $q > 1$ such that $1/p + 1/q = 1$, we can consider the case where J and J^* are generalized to

$$(J_{1,q}, J^*_{1,q}) = \left(\sum_{i,j}\|(Lx)_{i,j}\|_q, \iota_{C_{1,q}}\right), \tag{7}$$

where ι denotes the indicator function and

$$C_{1,q} = \left\{y \in X,\ \max_{i,j}\|u_{i,j}\|_p \le 1, \mathrm{div}(u) = y\right\}.$$

The standard case discussed earlier corresponds to the case $q = 2$, but alternative formulations using wavelet-based dual norms have also been explored [10].

C. Texture + Geometry + Noise Model

The previous formulation does not explicitly account for noise. To incorporate noise, various strategies have been proposed, among which the following proved to be particularly efficient [10], and can be described as follows:

$$\min_{(x,y,n)\in X^3} \frac{1}{2}\|z-x-y-n\|_2^2 + \lambda J(x) + J^*\Big(\frac{y}{\mu}\Big) + B^*\Big(\frac{n}{\delta}\Big), \tag{8}$$

where B^* is the dual norm of $B(x) = \|x\|_{B^1_{1,1}} = \|\Psi x\|_1$, $B^1_{1,1}$ being the Besov space with all parameters equal to 1, and corresponds to the l^1-norm of the wavelet coefficients of x (i.e., Ψ denotes the wavelet transform).

D. Comments on Existing Models and Generalization

At this stage, it is important to remark that $J = \|\cdot\|_{1,2}\circ L$, but if $q \neq 2$ in (7), projecting onto $C_{1,q}$ is not straightforward in general. This motivates the design of alternative minimization schemes that split the influence of the linear operator.

To be able to consider a wide variability of functions, we propose to generalize the formulation using a penalty of the form $f \circ L$ where f denotes a proper lower semi-continuous convex function and L is a linear operator mapping X to Y. This leads to the following generalized minimization problem:

$$\min_{x,y,n} \frac{1}{2}\|z-x-y-n\|_2^2 + \lambda f(Lx) + (f\circ L)^*\Big(\frac{y}{\mu}\Big) + B^*\Big(\frac{n}{\delta}\Big). \tag{9}$$

This formulation provides a flexible framework that can be adapted to different regularization terms and problem constraints.

III. Algorithmic Solutions

This section provides numerical schemes to solve (9). The involved functions being non-smooth it relies on proximal schemes [14], [15]. Our main contribution is the design of a novel algorithm based on primal-dual scheme involving post-composition.

A. Reminder

To facilitate the reading, we remind an extended formulation of Moreau decomposition [16], for $\gamma, \mu > 0$ and f proper, convex, lower-semi-continuous, for every $x \in X$,

$$\mathrm{prox}_{\gamma f^*(\cdot/\mu)}(x) = x - \frac{\gamma}{\mu}\mathrm{prox}_{\frac{\mu^2}{\gamma}f}\left(\mu(\gamma^{-1}x)\right). \tag{10}$$

This result is crucial for deriving efficient numerical schemes in our framework.

B. Forward-Backward Algorithm

The most common proximal iterations to minimize (9) rely on forward-backward algorithm, which yields for the kth iteration to

$$\begin{aligned} v_k &= x_k + y_k + n_k - z \\ y_{k+1} &= \mathrm{prox}_{\gamma(f\circ L)^*(\cdot/\mu)}(y_k - \gamma v_k) \\ x_{k+1} &= \mathrm{prox}_{\gamma\lambda(f\circ L)}(x_k - \gamma v_k) \\ n_{k+1} &= \mathrm{prox}_{\gamma B^*(\cdot/\delta)}(n_k - \gamma v_k). \end{aligned} \tag{11}$$

Equivalently, using Moreau's decomposition, this can be rewritten as:

$$\begin{aligned} v_k &= x_k + y_k + n_k - z \\ y_{k+1} &= y_k - \gamma v_k - \frac{\gamma}{\mu}\mathrm{prox}_{\frac{\mu^2}{\gamma}f\circ L}\left(\mu(\gamma^{-1}y_k - v_k)\right) \\ x_{k+1} &= \mathrm{prox}_{\gamma\lambda f\circ L}(x_k - \gamma v_k) \\ n_{k+1} &= n_k - \gamma v_k - \frac{\gamma}{\delta}\mathrm{prox}_{\frac{\delta^2}{\gamma}B}(\delta(\gamma^{-1}n_k - v_k)). \end{aligned} \tag{12}$$

In that context, $\mathrm{prox}_{f\circ L}$ can be computed at the cost of inner iterations. Indeed, $\mathrm{prox}_{f\circ L}(u) = u - L^\top\widehat{v}$ with

$$\widehat{v} = \arg\min_v \frac{1}{2}\|L^\top v - u\|_2^2 + f^*(v).$$

This dual minimization problem can be efficiently solved considering FISTA iterations [17]. In the iterative scheme (11), the convergence of the iterates to a solution of (8) is ensured for $\gamma < 1.99/\beta$ with $\beta = 3$ as $\frac{1}{2}\|z - x - y - n\|_2^2 = \frac{1}{2}\|z - [1\ 1\ 1][x, y, n]^\top\|_2^2$. Indeed, if one puts $A = [1\ 1\ 1]$ and $f(x, y, n) = \frac{1}{2}\|z - A[x, y, n]^\top\|_2^2$, then $\nabla f(x, y, n) = A^\top(A[x, y, n]^\top - z)$, thus $\|\nabla f(x, y, n) - \nabla f(x', y', n')\|_2 \leq \|A^\top A\|_2\|(x - x', y - y', n - n')\|_2$, with $A^\top A$ being a rank one matrix admitting 3 as non zero eigenvalue.

Remark. The initial algorithmic procedure established in [10] used alternating projections onto each variable. When x and n are fixed, Equation (8) is equivalent to projecting $z - x - n$ onto C_μ which is done using Chambolle algorithm [7]. This yields updates at the kth iterate:

$$\begin{aligned} y_{k+1} &= \mathrm{prox}_{(f\circ L)^*(\cdot/\mu)}(z - x_k - n_k) \\ x_{k+1} &= \mathrm{prox}_{\lambda(f\circ L)}(z - y_{k+1} - n_k) \\ n_{k+1} &= \mathrm{prox}_{B^*(\cdot/\delta)}(z - x_{k+1} - y_{k+1}). \end{aligned} \tag{13}$$

However, this procedure only guarantees convergence of the objective function, not for the sequence of iterates. In the numerical part, we thus focus on the standard forward-backward procedure.

C. Post-Composition Primal-Dual Algorithm

The second algorithmic strategy considered in this work takes advantage of the structure of (8) in order to facilitate the handling with linear operator and avoid inner iterations as required in the two previous schemes. Note that such a decomposition $J = f \circ L$ is valid for any types of norms introduced in Sec. II-B.

Since $(f \circ L)^* = L^* \triangleright f^* \colon t \mapsto \inf_{u,\, L^*u=t} f^*(u)$, where $\triangleright$ denotes the infimal post-composition operation (see, e.g., [18]–[20]), the minimization problem (8) rewrites

$$\min_{x,u,n} \frac{1}{2}\|z - x - L^*u - n\|_2^2 + \lambda(f \circ L)(x) + f^*\left(\frac{u}{\mu}\right) + B^*\left(\frac{n}{\delta}\right) \tag{14}$$

with $L^*u = y$, leading to the following reformulation:

Proposition 1. *Equation* (14) *can be solved using the following Condat-Vũ iterations:*

$$\begin{aligned} w_k &= x_k + L^*u_k + n_k - z \\ x_{k+1} &= x_k - \tau(w_k + L^*v_k) \\ u_{k+1} &= \mathrm{prox}_{\tau f^*(\cdot/\mu)}(u_k - \tau L w_k) \\ n_{k+1} &= \mathrm{prox}_{\tau B^*(\cdot/\delta)}(n_k - \tau w_k) \\ v_{k+1} &= \mathrm{prox}_{\sigma(\lambda f)^*}(v_k + \sigma L(2x_{k+1} - x_k)). \end{aligned} \tag{15}$$

Proof. The problem (14) can be equivalently written as

$$\min_{X=(x,u,n)} F(X) + G(X) + H(MX),$$

where

$$\begin{cases} F \colon X \mapsto \frac{1}{2}\|\Lambda(X) - z\|^2, \\ \Lambda \colon (x, u, n) \mapsto x + L^*u + n \\ G \colon X \mapsto f^*(\frac{u}{\mu}) + B^*(\frac{n}{\delta}) \\ H \colon v \mapsto \lambda f(v) \\ M \colon (x, u, n) \mapsto Lx. \end{cases}$$

The Condat-Vũ algorithm [11] can be applied within that framework and reads in that case

$$\begin{aligned} X_{k+1} &= \mathrm{prox}_{\tau G}(X_k - \tau\nabla F(X_k) - \tau M^* v_k) \\ v_{k+1} &= \mathrm{prox}_{\sigma H^*}(v_k + \sigma M(2X_{k+1} - X_k)). \end{aligned} \tag{16}$$

Since

$$\begin{cases} \nabla F \colon (x, u, n) \mapsto \Lambda^*(\Lambda(x, u, n) - z) \\ \qquad \text{with } \Lambda^* \colon y \mapsto (y, Ly, y) \\ M^* \colon v \mapsto (L^*v, 0, 0) \\ \mathrm{prox}_{\tau G} \colon (x, u, n) \mapsto (x, \mathrm{prox}_{\tau f^*(\cdot/\mu)}(u), \mathrm{prox}_{\tau B^*(\cdot/\delta)}(n)) \\ \mathrm{prox}_{\sigma H^*} = \mathrm{prox}_{\sigma(\lambda f)^*}. \end{cases}$$

Equation (16) is equivalent to

$$\begin{aligned} x_{k+1} &= x_k - \tau(x_k + L^*u_k + n_k - z) - \tau L^* v_k \\ u_{k+1} &= \mathrm{prox}_{\tau f^*(\cdot/\mu)}(u_k - \tau L(x_k + L^*u_k + n_k - z)) \\ n_{k+1} &= \mathrm{prox}_{\tau B^*(\cdot/\delta)}(n_k - \tau(x_k + L^*u_k + n_k - z)) \\ v_{k+1} &= \mathrm{prox}_{\sigma(\lambda f)^*}(v_k + \sigma L(2x_{k+1} - x_k)). \end{aligned}$$

Using Moreau decomposition one ends up with the proposed iterations. □

In practice, iterations (15) are computed using direct formulation as in the forward-backward algorithm (see Equation (12)). Note finally that the Lipschitz constant of the data term F is $\|\Lambda\|^2 = (2 + \|L\|^2)$. In order to ensure convergence, σ and τ must satisfy

$$\frac{1}{\tau} - \sigma\|L\|^2 > \frac{1}{2}(2 + \|L\|^2) \Leftrightarrow \tau < \frac{2}{2 + (1 + 2\sigma)\|L\|^2}. \tag{17}$$

IV. Results

In this section we evaluate first, the algorithmic behaviour of the proposed post-composition primal-dual algorithm compared to forward-backward steps and second, based on the proposed algorithm we analyze the impact of the regularization parameters onto decomposition performance.

A. Computational Time Evaluation

As a preliminary experiment, we implemented the two algorithms on the real 894×1400 image shown at the top Figure 1a, where we added a Gaussian white noise. A zoomed-in view of the region of interest, highlighted by a red frame in the image, is shown at the bottom of Figure 1a. In this example, we consider minimizing (9) with the following regularization parameters: $\lambda = 0.01$, $\mu = 0.2$ and $\delta = 0.01$, the value for the latter parameter being automatically computed [10]. Note that as the image is a colored image the minimization is performed on the three (red, green, and blue) channels independently.

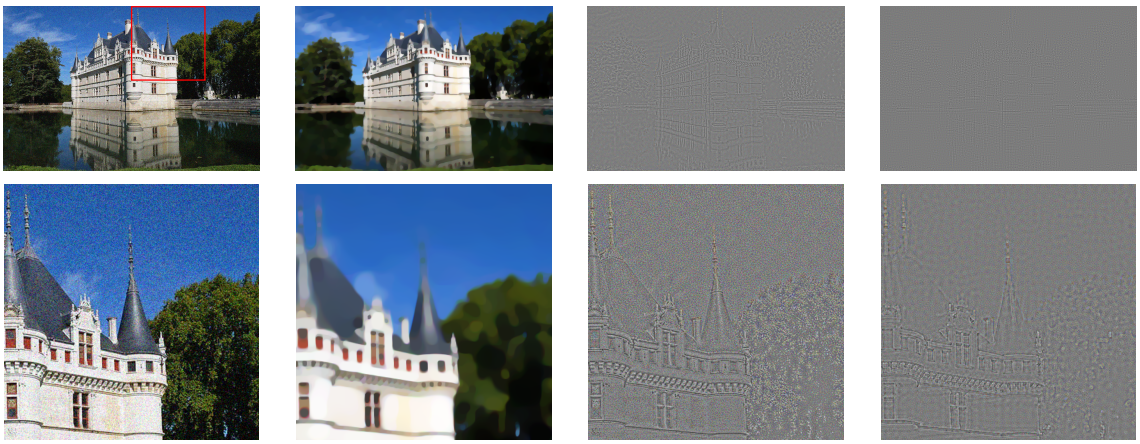

(a) (b) (c) (d)

Fig. 1: Output of post-composition primal-dual algorithm applied to a real image. Original image (a), estimated geometry (b), estimated texture (c), and estimated noise (d). The second row is a zoom in the area highlighted by a red frame in the top-left image.

Figures 1b to 1d depict the estimated geometry, texture and noise components obtained after convergence of the post-composition primal-dual algorithm. Although the ground truth is unknown, a qualitative assessment based on visual inspection shows that the geometry component consists essentially of piecewise constant regions, while the texture component captures fine image details (e.g., tree leaves).

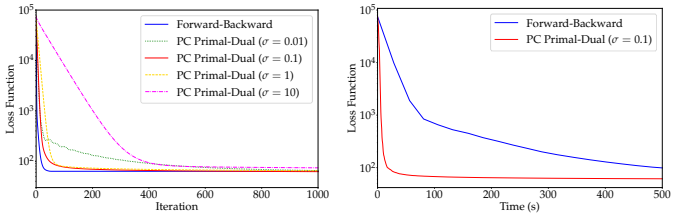

(a) Iteration convergence. (b) Computation time.

Fig. 2: Comparison of the speed of convergence of the minimization algorithms performed on the zoom-in view as the computation with FB was too long to process for the full image.

A comparison of the convergence speed for the two algorithms is shown in Figure 2. In particular, we have implemented the primal-dual algorithm for four different choices of σ parameter in (15) (namely, $\sigma = 0.01$, 0.1, 1 and 10). Each time, the step size τ was set to 0.9 times the upper bound given in Equation (17). Figure 2a shows convergence in terms of the number of iterations, while Figure 2b compares actual computational times. Although the forward-backward algorithm converges in very few iterations, it requires a significantly longer computational time. Indeed, because of the need for inner iterations to evaluate the proximal operator in (12), every update of x and y takes longer than in the post-composition primal-dual algorithm, where every update in (15) involves direct computations. In addition, we found that choosing $\sigma = 0.1$ results in the fastest convergence of the primal-dual algorithm among the tested values.

B. Role of the Regularization Parameters and Limitations

Equipped with the fast primal-dual post-composition algorithm, we can handle most exhaustive tests. To better understand the effect of regularization parameters on the estimates, we applied the proposed algorithm to the four toy images shown in Figure 3a. These images share the same geometric structure but differ in their texture patters. The first two images have periodic textures, the second image containing oscillations at twice the frequency of the first image. The last two textures are real images taken from the Brodatz's texture database [21]. In these experiments, the noise regularisation parameter δ was set to $\delta = 0.01$, while the geometry and texture regularization parameters λ and μ were varied. As a performance index, we computed the signal-to-noise ratios (SNR) for the geometry and texture components across different pairs of regularization parameters (λ, μ). The resulting SNR maps are shown in Figures 3b and 3c.

We observe that images with faster oscillations require a smaller μ to accurately capture the texture component. We also notice that the SNR of the texture component is only weakly dependent on λ. However, μ and λ cannot be chosen separately. We manually determined an optimal pair of regularization parameters, highlighted by red squares in the SNR maps. Figures 3d to 3f show the estimated geometry, texture and noise components for these optimal parameter values. As the texture complexity increases, even by choosing the optimal (λ, μ) parameters, the separation between geometry and texture becomes less accurate. This suggests the need for future improvements in optimization strategies to enhance decomposition quality.

V. Conclusion and Perspective

In this work, we propose a new and faster algorithmic scheme for texture and geometry decomposition, leveraging post-composition primal-dual iterations. This work paves the way to extended analysis on the choice of L for color imagery,

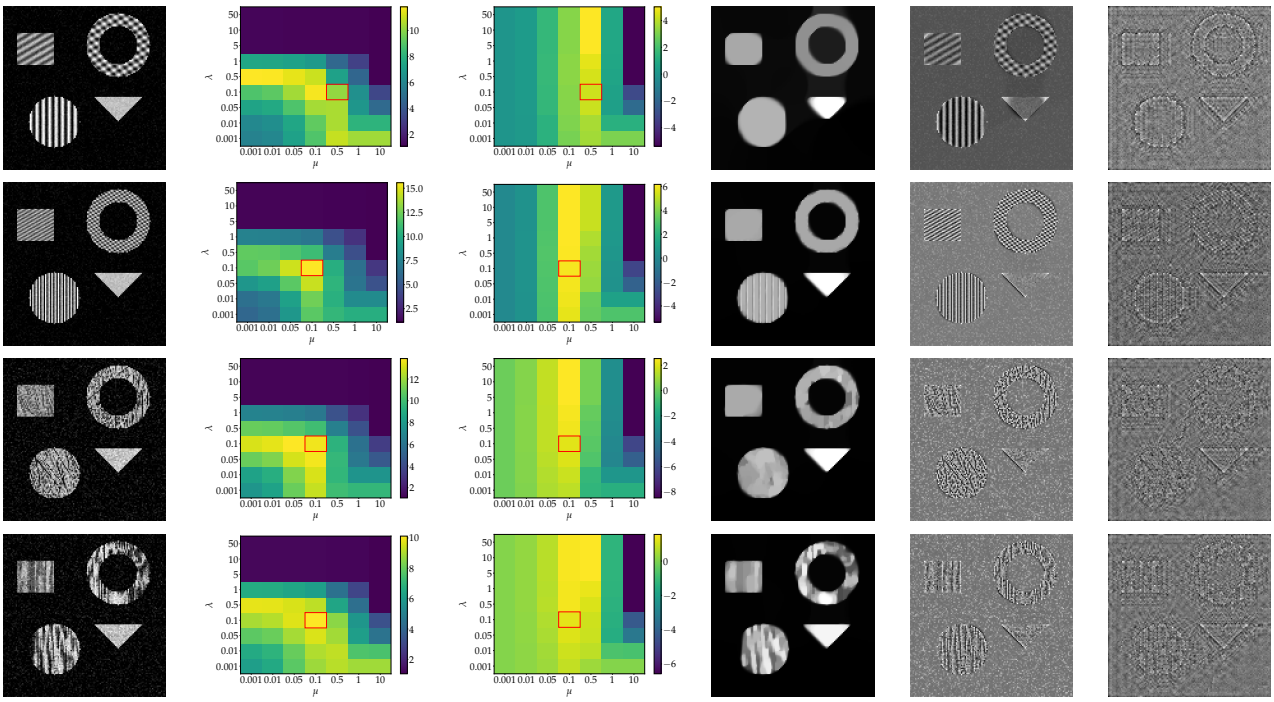

(a) (b) (c) (d) (e) (f)

Fig. 3: Quality of image decomposition in terms of SNR for four test images, evaluated as a function of the regularization parameters. Column (a) shows the original images, while columns (b) and (c) display the SNR maps for the geometry and texture components, respectively. The regularization parameters, selected manually, are highlighted with red squares. The corresponding estimated geometry, texture, and noise components are presented in columns (d) to (f).

but also to the design of unfolded schemes in order to learn more suitable norms for texture and geometry decomposition.

REFERENCES

[1] W. Dong, P. Wang, W. Yin, G. Shi, F. Wu, and X. Lu, "Denoising prior driven deep neural network for image restoration," *IEEE Trans. Pattern Anal. Match. Int.*, vol. 41, no. 10, pp. 2305–2318, 2018.

[2] K. Zhang, W. Zuo, S. Gu, and L. Zhang, "Learning deep CNN denoiser prior for image restoration," in *Proc. IEEE Comput. Soc. Conf. Comput. Vis. Pattern Recognit.*, pp. 3929–3938, 2017.

[3] V. Monga, Y. Li, and Y. C. Eldar, "Algorithm unrolling: Interpretable, efficient deep learning for signal and image processing," *IEEE Signal Processing Magazine*, vol. 38, no. 2, pp. 18–44, 2021.

[4] L. I. Rudin, S. Osher, and E. Fatemi, "Nonlinear total variation based noise removal algorithms," *Physica D: Nonlinear Phenomena*, vol. 60, no. 1, pp. 259–268, 1992.

[5] Y. Meyer, *Oscillating Patterns in Image Processing and Nonlinear Evolution Equations: The Fifteenth Dean Jacqueline B. Lewis Memorial Lectures*. American Mathematical Soc., 2001.

[6] J.-F. Aujol, G. Aubert, L. Blanc-Féraud, and A. Chambolle, "Image Decomposition into a Bounded Variation Component and an Oscillating Component," *Journal of Mathematical Imaging and Vision*, vol. 22, no. 1, pp. 71–88, 2005.

[7] A. Chambolle, "An Algorithm for Total Variation Minimization and Applications," *J. Math. Imag. Vis.*, vol. 20, no. 1, pp. 89–97, 2004.

[8] L. A. Vese and S. J. Osher, "Modeling Textures with Total Variation Minimization and Oscillating Patterns in Image Processing," *J. Sci. Comput.*, vol. 19, no. 1, pp. 553–572, 2003.

[9] L. M. Briceño-Arias, P. L. Combettes, J.-C. Pesquet, and N. Pustelnik, "Proximal algorithms for multicomponent image recovery problems," *J. Math. Imag. Vis.*, vol. 41, pp. 3–22, Sep. 2011.

[10] J.-F. Aujol and A. Chambolle, "Dual norms and image decomposition models," *International journal of computer vision*, vol. 63, pp. 85–104, 2005.

[11] L. Condat, "A primal–dual splitting method for convex optimization involving Lipschitzian, proximable and linear composite terms," *Journal of Opt. Theory and Applications*, vol. 158, no. 2, pp. 460–479, 2013.

[12] B. C. Vũ, "A splitting algorithm for dual monotone inclusions involving cocoercive operators," *Adv. Comput. Math.*, vol. 38, pp. 667–681, Apr. 2013.

[13] J.-F. Aujol, G. Gilboa, T. Chan, and S. Osher, "Structure-Texture Image Decomposition—Modeling, Algorithms, and Parameter Selection," *Int. J. Comput. Vis.*, vol. 67, no. 1, pp. 111–136, 2006.

[14] H. H. Bauschke and P. L. Combettes, *Convex Analysis and Monotone Operator Theory in Hilbert Spaces*. New York: Springer, 2017.

[15] P. L. Combettes and J.-C. Pesquet, "Proximal splitting methods in signal processing," in *Fixed-Point Algorithms for Inverse Problems in Science and Engineering* (H. H. Bauschke, R. S. Burachik, P. L. Combettes, V. Elser, D. R. Luke, and H. Wolkowicz, eds.), pp. 185–212, New York: Springer-Verlag, 2011.

[16] J. J. Moreau, "Fonctions convexes duales et points proximaux dans un espace hilbertien," *Comptes rendus hebdomadaires des séances de l'Académie des sciences*, vol. 255, pp. 2897–2899, 1962.

[17] A. Beck and M. Teboulle, "A fast iterative shrinkage-thresholding algorithm for linear inverse problems," *SIAM J. Imaging Sci.*, vol. 2, no. 1, pp. 183–202, 2009.

[18] L. M. Briceño-Arias and N. Pustelnik, "Infimal post-composition approach for composite convex optimization applied to image restoration," *Signal Processing*, vol. 223, p. 109549, 2024.

[19] H. H. Bauschke and P. L. Combettes, *Convex Analysis and Monotone Operator Theory in Hilbert Spaces*. CMS Books in Mathematics/Ouvrages de Mathématiques de la SMC, Cham: Springer, second ed., 2017.

[20] S. R. Becker and P. L. Combettes, "An algorithm for splitting parallel sums of linearly composed monotone operators, with applications to signal recovery," *J. Nonlinear Convex Anal.*, vol. 15, no. 1, pp. 137–159, 2014.

[21] P. Brodatz Textures, "A photographic album for artists and designers," 1966.